Riedl, *Appl. Surf. Sci.*, **104-105**, 61 (1996).
19. G. Hodes and M. Grätzel, *Nouv. J. Chim.*, **8**, 509 (1984).
20. A. J. Bard, *J. Phys. Chem.*, **86**, 172 (1982).
21. S. Södergren, A. Hagfeldt, J. Olsson, and S.-E. Lindquist, *J. Phys. Chem.*, **98**, 5552 (1994).
22. G. Hodes, I. D. J. Howell, and L. M. Peter, *J. Electrochem. Soc.*, **39**, 3136 (1992).
23. W. J. Albery and P. N. Bartlett, *J. Electrochem. Soc.*, **131**, 315 (1984).
24. See, for example, J.-C. Vial and J. Derrien, *Porous Silicon Science and Technology*, Springer-Verlag, Berlin (1995).
25. L. E. Brus, *Phys. Rev.*, **B53**, 4649 (1996).
26. G. Hodes, in *Proceedings of the 6th Sede Boker Symposium on Solar Electricity Production*, Ben-Gurion National Solar Energy Center, D. Faiman, Editor, pp. 157-161, Nov 1994.
27. R. Könenkamp, R. Henninger, and T. Hoyer, *J. Phys. Chem.*, **97**, 7328 (1993).
28. A. Many, Y. Goldstein, and N. B. Grover, *Semiconductor Surfaces*, 2nd ed., North-Holland, Amsterdam (1971).
29. V. M. Buimistrov, A. P. Gorban, and V. G. Litovchenko, *Surf. Sci.*, **3**, 445 (1965).
30. H. von Känel, E. Kaldis, P. Wachter, and H. Gerischer, *J. Electrochem. Soc.*, **131**, 77 91984).
31. M. H. Hecht, *Phys. Rev.*, **41**, 7918 (1990) and *J. Vac. Sci. Technol.*, **B8**, 1018 (1990).
32. R. Schlaf, A. Klein, C. Pettenkofer, and W. Jaegermann, *Phys. Rev.*, **48**, 14242 (1993).
33. M. G. Bawendi, P. J. Carroll, W. L. Wilson, and L. E. Brus, *J. Chem. Phys.*, **96**, 946 (1992).
34. M. G. Bawendi, W. L. Wilson, L. Rothberg, P. J. Carroll, T. M. Jedju, M. L. Steigerwald, and L. E. Brus, *Phys. Rev. Lett.*, **65**, 1623 (1990).
35. M. Nirmal, C. B. Murray, and M. G. Bawendi, *Phys. Rev.*, **B50**, 2293 (1994).
36. A. P. Alivisatos, A. Harris, N. Levinos, M. L. Steigerwald, and L. E. Brus, *J. Chem. Phys.*, **89**, 4001 (1989).
37. I. A. Davydov, L. P. Strakhov, and S. L. Tselishchev, *Sov. Phys. Semicond.*, **26**, 89 (1992). [*Fiz. Tekh. Poluprovodn.*, **26**, 159 (1992)].
38. M. O'neil, J. Marohn, and G. Mclendon, *J. Phys. Chem.*, **94**, 4356 (1988).
39. E. Eychmüller, A Hässelbarth, L. Katsikas, and H. Weller, *Ber. Bunsen-Ges. Phys. Chem.*, **95**, 79 (1991).
40. M. L. Steigerwald and L. E. Brus, *Acc. Chem. Res.*, **23**, 183 (1990).
41. X. Tong, D-P. Xu, W-H. Su, L.-Z. Xiao, S-T. Li, and L. Han, *AIP Conf. Proc.*, **309**, 1271 (1994).
42. D. Meissner, I. Lauermann, R. Memming, and B. Kastening, *J. Phys. Chem.*, **92**, 3484 (1988), and references therein.

Ion Drift Processes in Pyrex-Type Alkali-Borosilicate Glass during Anodic Bonding

Petra Nitzsche, Klaus Lange,[a] Bernd Schmidt, Stephan Grigull, and Ulrich Kreissig

Forschungszentrum Rossendorf, Institut für Ionenstrahlphysik und Materialforschung, D-01314 Dresden, Germany

Berthold Thomas and Karin Herzog

Institut für Analytische Chemie, TU Bergakademie Freiberg, D-09596 Freiberg, Germany

ABSTRACT

Electric field induced ion drift processes in alkali-borosilicate glasses play a key role in the silicon-glass or metal-glass compound formation in anodic bonding processes. By means of ex situ and in situ ion-beam analysis, which allows a quantitative depth profiling of different elements, the formation of anodic, alkali depleted glass layers and of oxygen enriched interface layers was investigated. Drift rates and depletion layer thicknesses were determined in dependence of the process temperature, bias, and drift time. The drift behavior of cations, including sodium, potassium, calcium, aluminum, and hydrogen, was examined. In addition, the drift of oxygen ions toward the compound interface was investigated. The absence of nonbridging oxygen in the investigated glass, verified by nuclear magnetic resonance investigations, gives rise to the conclusion that the drift behavior of oxygen ions depends mainly on the composition of the "leached" glass surface layer. The results confirm the anodic oxidation as the main mechanism responsible for the interface chemistry. The oxygen enrichment (oxidation) of the metal or silicon anode can be described by a reciprocal logarithmic equation.

Introduction

Anodic bonding[1] has been established as a standard process in microsystem technology for joining silicon and glass.[2] For glass-to-metal sealing it is a promising technique, although still only occasionally employed. Anodic bonding results in a high bonding reliability at relatively low process temperatures below the glass transition point. This holds especially for the bonding of strongly bent silicon wafers. However, in spite of broad applications and diverse scientific work, the mechanism of anodic bonding is not yet clarified in detail. In particular a better knowledge of drift rate processes would be useful to optimize anodic bonding steps with respect to contradictory requests as, for example, low thermomechanical stress and quick, reliable bonding.[3]

A key mechanism of anodic bonding is the thermal and, possibly, electric-field assisted activation of ions and their drift in the electric field applied during bonding.[4-6] Due to the low thermal activation energies of alkali ions in glasses, their drift is recognized to determine the rate of bonding in general.[6] For blocking anode materials (e.g., silicon or aluminum), that is, for negligible migration of cations from the anode material into the glass, this drift results in a polarized depletion layer in the glass at the compound interface.[4,6-8] The high electric field strength within the depletion region leads to a strong electrostatic attraction at the planar interface and, therefore, to an intimate contact necessary for reliable, laterally homogeneous bonding. A field-assisted movement of stronger bound atoms can become possible. In particular, the drift of oxygen ions and subsequent anodic oxidation of silicon was discussed as a reaction pathway which governs the formation of chemical bonds at the compound interface.[5,6] Direct evidence for the anodic oxidation as the essential interface reaction in anodic glass-silicon-bonding was recently given by Baumann et al.[2]

Altogether, a better knowledge of the ion drift processes will be a significant step for understanding anodic bonding. Therefore, investigations of mobile species and their con-

[a] Present address: Physikalisches Institut, Universität Bern, CH-3012 Bern, Switzerland.

centrations inside the depletion layer are of great importance. Until now, ion scattering spectroscopy (ISS),[8,9] Auger electron spectroscopy (AES),[10] secondary ion and secondary neutral mass spectroscopy (SIMS, SNMS),[11,12] as well as electron-probe microanalysis (EPMA),[4,8-10,13] and X-ray photoelectron spectroscopy (XPS)[14] have been used for this purpose. However, electron-microprobe and XPS studies using cross sections of pretreated samples were limited by the poor depth resolution achieved with these methods. The other methods are in principle only surface sensitive, too, so that depth profiles have to be determined by gradually sputtering the surface, which might distort the profiles to be measured. Thus, quantitative depth profiling of alkali containing glasses is still a difficult problem. Therefore, previous studies of the depletion layer formation were mainly based on the interpretation of measured external bonding current responses[4,5,7,8,15] rather than on the compositional analysis of the depletion layer.

In the present work, the ion drift behavior is investigated by quantitative depth profiling using in situ elastic recoil detection analysis (ERDA).[16,17] ERDA is particularly well suited for the objectives of the studies described here because of its ability to measure the depth resolved contents of various atomic components of technical glasses simultaneously[17,18] without gradually sputtering. Besides, the nondestructive character of ERDA is a key point for the in situ analysis of drift processes during anodic bonding.

Experimental

The sodium-borosilicate glass Tempax (Schott no. 8330, almost identical with Pyrex, Corning no. 7740), which is widely used in microsystem technology because of its thermal expansion coefficient being close to that of silicon, was investigated. Because the ion drift processes in anodic bonding are essentially restricted to processes within the glass and depend only marginally on the anode material or interface chemistry, idealized model samples were used alternatively to real compound targets for the in situ ion-beam studies. These samples consisted of anodic and cathodic aluminum or silicon coated glass (see Fig. 1a). The anodic layer thickness was made small enough (typically 30 nm thick) to study the ion drift processes at the anode without significant reduction of the analyzable depth.

The additional cathode coating of the glass samples ensures planar contacts and, therefore, a well-defined, laterally homogeneous electric field distribution during drift treatments. The sample areas and thicknesses were about 2 cm^2 and 0.8 mm, respectively. For ex situ ERDA, glass samples were prepared by drift treatments using a commercial anodic bonder (AB400, ATV Technologie GmbH). Details of the experimental procedure have already been given elsewhere.[18] In the case of the in situ investigations the glass samples were glued to a copper plate (about 2.5 cm diam, 1.5 mm thickness) heated by an ohmic heating element (Boralectric, Advanced Ceramics). The temperature was measured by a jacket thermocouple inserted sideways into a narrow cavity of the copper plate. The electrically and thermally conductive carbon tape used for the sample mounting guarantees an optimal thermal contact between the copper cathode and the glass sample even under the high-vacuum conditions necessary for ERDA. The temperature as well as the heating current, the drift voltage, and current were monitored as a function of the time using a data logger (Fluke Hydra 2620A). The influence of the residual gas pressure in the scattering chamber on the drift processes was tested by a series of independent experiments, because such an influence is discussed in connection with the observation of pressure-dependent variations of the bonding rate (see, for example, Ref. 3). The present experiments have clearly shown that the drift current is not influenced by the gas itself but indirectly by thermal effects like a reduced temperature in the glass due to insufficient thermal coupling at low ambient pressures. In particular, a decrease of the drift current by a factor of 10 during evacuation of the scattering chamber from 10^{3} mbar up to 10^{-4} mbar was observed in the case of glass

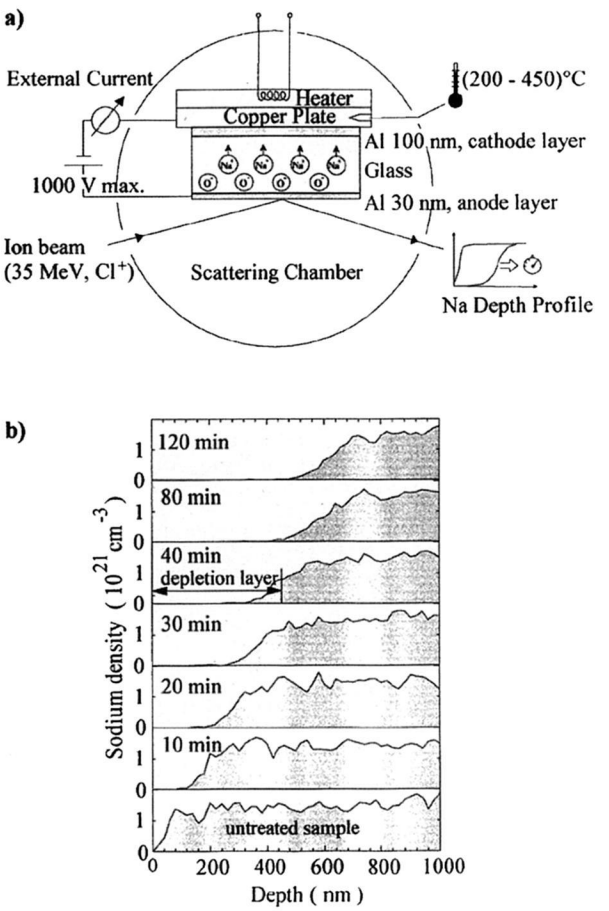

Fig. 1. Experimental arrangement for in situ ERDA and simultaneously external drift current measurement (a), and formation of the sodium depletion layer in an Al coated Tempax sample during an in situ drift sequence at a temperature of 210°C and a drift voltage of 250 V (b).

samples, which were only clamped on the flat, polished copper plate without adhesive. However, no significant change of the drift current was found in the same ambient pressure range in the case of sample mounting using adhesive carbon tape.

For ERDA with heavy ions,[16] projectile ions with energies of about 1 MeV/amu strike the target surface at small angles of incidence (in this work 7 and 15°, respectively) and the recoiling ions are detected under forward-scattering angles (here 30°) and discriminated with respect to their energy and atomic number or mass (see Fig. 1a). For the present experiments, the ERDA measurements were mainly carried out at the Rossendorf 5 MV tandem accelerator using 35 MeV ^{35}Cl incident ions. At a given projectile energy, the analyzable depth for the different elements depends on both the detection system and scattering geometry.[17] In the case of the Bragg ionization chamber mainly used for the ex situ experiments, the analyzable depth varies with the atomic number of the target recoils and was for sodium about 350 and 180 nm for incidence angles of 15 and 7°, respectively. The time-of-flight detector developed especially for the in situ glass analysis allows the detection of sodium recoils emitted from depths up to about 1000 nm. To increase the analyzable depth additionally, some supplementary ex situ measurements of Tempax with 210 MeV ^{127}I as projectiles were made using the 14 MV tandem accelerator at the University of Munich.

Possible ion-beam effects, in particular for the in situ drift experiments, were investigated by comparing results of ERDA measurements after identical drift treatments at which the Cl beam was either switched on or switched off. For a beam switched on during the drift treatment the sodium drift rate was observed to be up to five times high-

er than the drift rate determined from the drift yield after a corresponding treatment without ion beam. However, from the correlation between Na drift and external drift current measurements these effects could be concluded to be mainly due to local sample heating by the analyzing beam. For these reasons, most of the in situ experiments were performed as sequences of analysis and drift periods with sufficient breaks in between. Possible relaxation effects during the analysis periods and breaks without external drift voltage but still heated sample are discussed in connection with ion drift results.

Furthermore, ^{11}B, ^{27}Al, ^{29}Si, and ^{1}H nuclear magnetic resonance (NMR) spectra were recorded at a magnetic field B_0 = 7.05 T using a Brucker MSL 300 spectrometer for investigations of chemical coordination of B, Al, Si, O, and H in the glass.[19]

Results and Discussion

Sodium drift.—The formation of the Na depletion layer could be observed in a depth range of about 1 μm. Figure 1b shows the evolution of this layer during a given sequence of drift treatments at a fixed drift temperature of 210°C and a drift voltage of 250 V. The untreated reference sample is slightly depleted of sodium within a depth range of about 70 nm from the Al glass interface. Alkali depleted near surface glass layers have been often observed and were explained by leaching effects on the glass surface due to indiffusion of water from the ambient.[20] The measured Na density of $(1.41 \pm 0.15)\cdot 10^{21}$ cm^{-3}, corresponding to (2.2 ± 0.3) atom %, are in agreement with the concentration given by the glass manufacturer (2.4 atom % given by Schott/Desag). On account of the depletion layer in the untreated sample (undrifted reference sample) and the continuous transition of the Na concentration at the edge from the depletion layer to the constant bulk concentration, the depletion layer thickness was defined as the difference between the two depths measured in the sample after a certain treatment and in the reference sample. The depth values were taken for the local Na concentration at half of the bulk concentration (see Fig. 1b). The atomic area densities obtained in that manner can be interpreted as integrated charge currents per area unit and give directly the totally transferred charges (Na^+) during the drift steps. An alternative possibility of the Na depletion layer thickness determination can be given by the difference between the integrals of the depth profiles.

Figure 2 presents the development of the Na depletion layer thickness in dependence on drift time and temperature at a constant drift voltage of 250 V for all measurements. The saturation effect which is to be expected due to the decreasing electric field strength in the increasing depletion layer was obtained for all Na drift measurements. If Na is the only activated charge carrier and if a finite energy threshold for a stable Na shift exists, the saturation thicknesses should be dependent only on the external drift voltage. The alkali drift rates were observed to decrease at temperatures below typical temperatures for anodic bonding of about 400°C. At temperatures $T \geq 400$°C the drift rate of Na is too high and leads to depletion layer thicknesses of > 1 μm, which could not be investigated using 35 MeV ^{35}Cl incident ions. For example, at 400°C and 500 V the Na depletion layer thickness is about 1.5 μm after 15 min drift time, as measured by ex situ ERDA using 210 MeV I ions at the Munich 14 MV tandem accelerator. At temperatures and voltages applied usually during anodic bonding the enhanced alkali drift rate results in depletion layer thicknesses of some micrometers.

To investigate a possible influence of the experimental procedure on the depletion layer formation (sequences of drift and analysis periods) experiments were performed by varying the time steps using a constant drift voltage and drift temperature. However, no significant influence was found. In addition, a purely diffusive modification of the Na profiles was checked at a temperature of about 400°C. Within 30 min the profiles were observed to remain undisturbed without an external electrical field. Finally, the

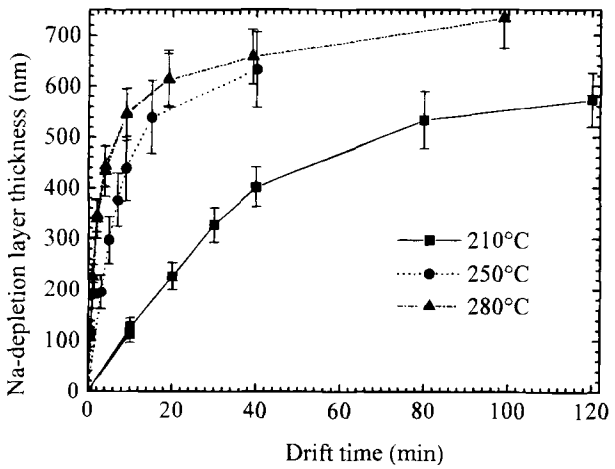

Fig. 2. Sodium depletion layer thicknesses in Tempax as a function of the drift time at various temperatures and a drift voltage of 250 V. Different drift temperatures are indicated by different symbols.

possibility of a backward drift of sodium ions due to the internal polarization field in the depletion layer was investigated in situ at constant temperatures after switching off the voltage and was found to be negligible.

The activation energy E_a of the sodium drift was calculated from the drift time intervals necessary to deplete a fixed near surface layer of 120 nm thickness. The corresponding Arrhenius plot is shown in Fig. 3. The natural logarithm of the drift rate shows a linear dependence on the inverse temperature, that is, the drift rate is proportional to a Boltzmann factor. The activation energy E_a can be derived from the slope of the linear fit to the data points in Fig. 3 and was determined to be $E_a = (0.97 \pm 0.14)$ eV. In addition, the sodium drift current shows an ohmic behavior. The drift-activation energy can be compared to results from temperature dependent electrical conductivity measurements. In this comparison, it must be assumed that the conductivity is dominated by sodium ions as charge carriers, which is described later. For Pyrex an activation energy of E_a = 0.88 eV was published.[21] For purely thermal sodium diffusion in Pyrex an activation energy E_a = 0.80 eV was measured by Wilson and Carter[22] using radioactive ^{22}Na tracer method. Therefore, E_a values for diffusion and drift processes are comparable, indicat-

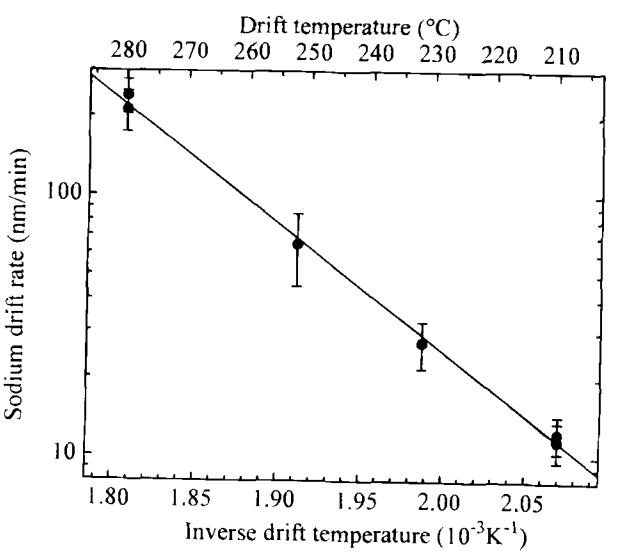

Fig. 3. Arrhenius plot describing the thermal activation of the drift of sodium in Tempax samples treated at a drift voltage of 250 V.

ing the minor role of the electric field for the drift activation of Na^+.

Drift of potassium, calcium, and aluminum ions.—The drift of potassium and calcium in Tempax was investigated using the time-of-flight telescope within a depth range of up to a few hundred nanometers. However, the mass resolution of the detection system was not good enough to discriminate the two species from each other. After long drift periods K and Ca were clearly missing in the near surface region of the glass at the anodic side. In addition, a pile-up was observed at the Na depletion layer edge. This behavior indicates that the drift of these elements is correlated to the sodium drift. A similar behavior for other glasses is already known from the literature.[9] Due to the small concentration of K and Ca (only 10% of the Na concentration) their contribution to the drift current is assumed to be quite small compared to sodium.

The analysis of aluminum in the samples was limited to a depth range of about 50 nm in the in situ experiment. Therefore, Tempax samples were also investigated ex situ at the Munich 14 MV tandem accelerator using 210 MeV I ions. Only for high temperatures and voltages (T_d = 400°C and U_d = 400 V) was a drift of Al ions from the top layer into the glass bulk material detected. However, the number of Al ions displaced per unit area turned out to be relatively small compared to the number of Na ions under identical conditions. The Al displacement was limited to the Na depletion layer range. Wallis has described such a behavior of Al ions in the presence of large electric fields in Pyrex.[7]

External drift current measurements.—In most experiments on anodic bonding, the bonding process itself was monitored or characterized by the current measured in the external circuit.[3,7] For the present work, a comparison between the displaced charge taken from current measurement in the external circuit and the displaced atoms per unit area determined by ERDA provides information about the contribution of the different ion species to the total drift current. From the number of displaced atoms per unit area, the totally displaced charge was calculated, with the assumption that the corresponding atoms are singly charged. Figure 4 presents the area density of charges transferred in the external circuit and the displaced charge area density determined from ERDA depth profiles of different elements as a function of the drift time at different temperatures and drift voltages. The inset shows the displaced charge area densities after long drift times at a low temperature of 210°C and a drift voltage of 250 V. Here, the closed symbols describe the transferred charge taking into account only the drifted sodium ions. In this case, the external current can be almost completely explained by the drift of sodium. The slight difference between the two transferred charges at the end of the long drift process can be attributed to the drift of potassium and calcium. A high charge deficit that means a high difference between the external current and the sodium current was observed after drift sequences at higher drift voltage (500 V) and drift temperature (400°C). From in situ measurements and the ex situ measurements at the Munich accelerator, we concluded that the aluminum drift from the top layer (anode) into the polarization layer can be neglected. The locally displaced Al charge of 5 mC cm^{-2} obtained from in situ ERDA after the complete drift sequence is quite small compared to the charge deficit of about 30 mC cm^{-2}. A maximum charge contribution of only 7 mC cm^{-2} can be calculated for the drift of K and Ca. Therefore, the deficit between the external electric current and the cation current at high drift voltages (and high temperatures) cannot be explained if the drift of anions, especially that of oxygen, is not taken into consideration.

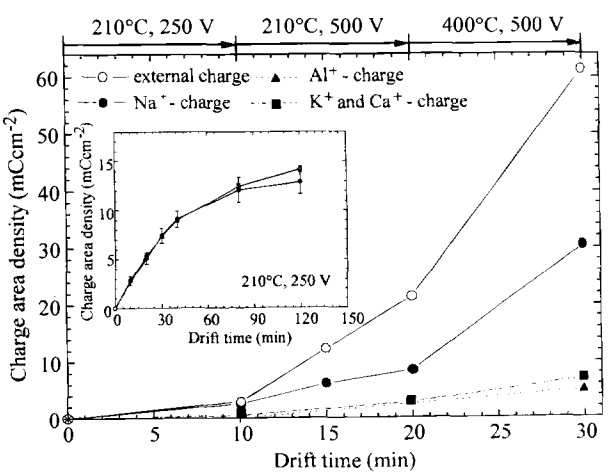

Fig. 4. Transferred charge area density in the external current circuit (open symbols) and displaced charge area densities of different elements as determined from ERDA measurements (closed symbols) as a function of drift time at different drift temperatures and drift voltages. The contribution of aluminum at the final stage was determined from ex situ experiments.

Oxygen and hydrogen drift.—It is generally realized that anodic bonding of Tempax (or Pyrex) and silicon using needle electrodes is not very efficient and not reliable at temperatures below 350–400°C and usual bond voltages of 500–1000 V.[2,3] Nevertheless, using evaporated full area cathode electrodes to create homogeneous electric field distribution reliable glass silicon compounds with high strength have been produced at 325°C and a bond voltage of 250 V.[23] Assuming that the chemical compound formation at the interface requires an anodic oxidation process, a drift of oxygen toward the glass-anode interface has to be expected even at temperatures lower than 350°C. From a more practical view of anodic bonding, ERDA investigations are of great interest in the temperature range around 300°C. This is because the thermal strain difference between silicon and Tempax below 350°C is quite small and is zero at T = 280°C. For the present quantitative investigations of the oxygen drift and the neccessary oxygen depth profiling thicker Al electrodes (80–100 nm) were used to separate the oxygen peak at the Al surface from the oxygen edge at the Al glass interface. In addition, a smaller incident angle of the ion beam (7° instead 15°) was chosen to enhance the resolution. The experimental depth profiles in Fig. 5 show a significant oxygen drift even at the relatively low temperature of 280°C and a drift voltage of 250 V. The small peak at the surface (d = 0 nm) can be assigned to the native Al_2O_3 at the Al electrode surface. The oxygen edge has been displaced into the Al top layer up to 4 and 8 nm at T_d = 280°C, U_d = 250 V, and T_d = 400°C, U_d = 500 V, respectively. Drift time dependent oxygen area densities, which are displaced to the Al

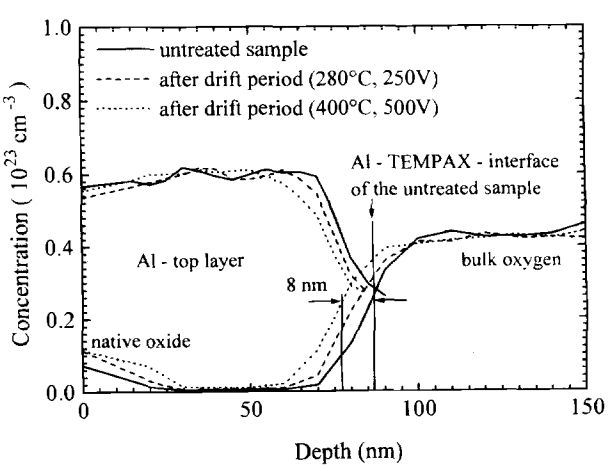

Fig. 5. Depth profiles of oxygen and aluminum demonstrating the drift of oxygen to the 85 nm thick Al electrode at different drift voltages and drift temperatures.

top layer at 320°C and 250 V, are plotted in Fig. 6. The drift rate of oxygen was found to be high at the initial state of the drift ($t < 5$ min) and saturates at longer drift times. The "oxidized" Al layer thickness, which was obtained from the shift of the oxygen edge, agrees with the calculated thickness within the experimental errors assuming that all drifted oxygen atoms are consumed for the Al_2O_3 formation at the Al glass interface.

To test the applicability of the results for the Al coated glass samples to silicon glass compounds an in situ experiment at T_d = 350°C and U_d = 500 V was carried out with a 100 nm thick anodic layer of sputtered amorphous silicon (a-Si). For the a-Si-glass sample, a shift of the oxygen edge up to 4 nm was observed. Therefore, an oxidation of the anode material at the glass interface can also be assumed for the silicon-glass compound. The stoichiometry of the 4 nm thick silicon oxide as well as of the 8 nm thick aluminum oxide layer has not been investigated, however, their composition can be assumed to be that of $Si_xO_yH_z$ and $Al_xO_yH_z$, respectively. For thermal treatments (280 and 350°C 40 min each) without external drift voltage, no oxygen displacement was found. In summary, the chemical compound formation in anodic bonding has to be explained mainly by an electric field assisted process and turned out to be not purely thermally activated.

Supposing that the measured amount of drifted oxygen atoms results in an oxidation rate, the oxide layer thickness d as a function of time follows qualitatively the reciprocal logarithmic relation $d(t) = 1/[A - B\cdot\ln(t)]$, where A and B are constants. This equation based on the theory of Cabrera and Mott[24] describes the purely field-assisted oxide growth and the oxidation mechanism at low temperatures (room temperature, 20°C) as well as the anodic oxidation of metals (e.g., Al) in wet electrolytes.[24] The formation of the oxide layer thickness is limited by the exponentially decreasing bonding current (ion current through the oxide layer) with increasing layer thickness and the decreasing drift rate from the oxygen source because of the decreasing electric field strength.

The area density of oxygen atoms, which were displaced from the glass bulk to the anodic top layer, was calculated from different oxygen depth profiles and is equivalent to a transferred charge area density of 3.2 mC cm^{-2} at 240°C and 4.2 mC cm^{-2} at 320°C after corresponding drift times. As can be seen, for the data shown in Fig. 7 the above mentioned charge deficit between the transferred charge density in the external circuit and the displaced charge area density as determined from ERDA measurements can be approximately explained by the drift of oxygen.

The question concerning the source of the observed mobile oxygen, which may be the weakly chemical bonded

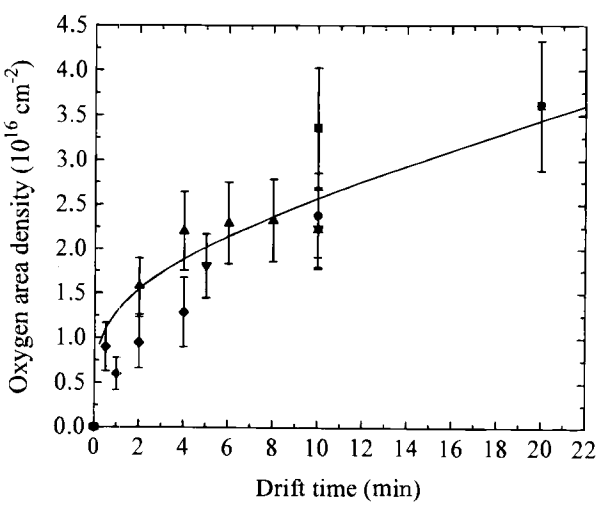

Fig. 6. Displaced oxygen area density into the Al top layer at 320°C and 250 V determined from five drift experiments as function of the drift time.

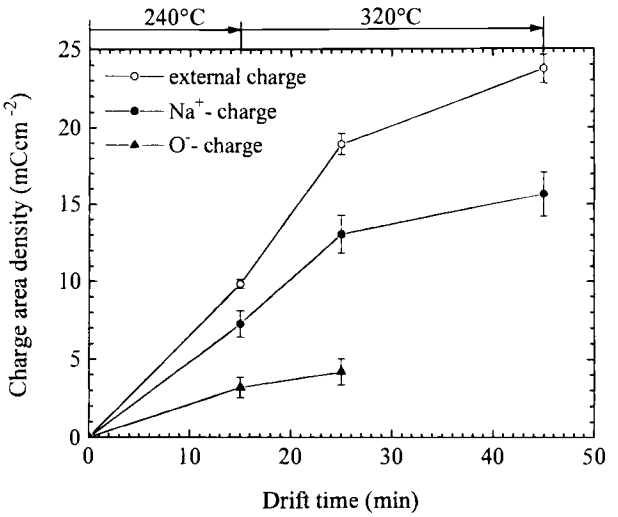

Fig. 7. External transferred charge density (open symbols) in comparison with the displaced Na^+ and O^- charge densities (closed symbols) for a drift sequence at a constant voltage of 250 V. After the first step the temperature was increased from 240 to 320°C.

nonbridging oxygen (NBO) in the glass matrix,[25] was solved by NMR investigations of Tempax. The NMR measurements give information about the chemical bonding behavior of the ^{1}H, ^{11}B, ^{27}Al, and ^{29}Si in correlation with oxygen. In binary borate glasses and ternary sodium borosilicate glass systems, the ^{11}B NMR absorption spectra have been in particular used to determine the fraction of $[BO_4]^-$ units, the fraction of $[BO_3]$ units with one or two NBO, and the fraction of $[BO_3]$ units with all bridging oxygen.[26]

Figure 8 presents an example of a magic angle spinning (MAS) NMR spectrum. The ^{11}B spectrum was recorded at an operating frequency of 96.3 MHz. Short pulses of 2 μs duration have been used with a repetition time of 5 s and a pulse angle of about 25°. The chemical shift is referenced against BF_3OEt_2. The ^{11}B-MAS-NMR spectrum shows two distinct features: (*i*) a narrow line due to $[BO_4]^-$ tetraeders, and (*ii*) a broad line due to planar $[BO_3]$ units with three bridging oxygens. From the total boron concentration of $2.1\cdot10^{21}$ cm^{-3} in Tempax glass and the peak areas in the right inset in Fig. 8 a ratio $[BO_4]^-:[BO_3] = 1:3$ was determined that is consistent with data from Yun and Bray[26] for sodium borosilicate glasses with $R = [Na_2O]/[B_2O_3] < 0.5$ ($R = 0.33$ for Tempax). Furthermore, from the broad unstructured ^{29}Si-MAS-NMR peak it was also concluded that in the Tempax glass network only Q^4_m-groups ($[SiO_4]$-tetraeder) are existent. These groups are partially coupled to B and Al atoms. An evidence for the existence of NBO was not found. The established absence of NBO in Tempax is in aggreement with results given by Milberg et al.[27] for sodium borosilicate glasses with $R < 0.5$. From the present measurements we conclude that due to the glass composition the whole aluminum and a part of boron have a coordination number of four and sodium serves for the charge compensation of the $[AlO_4]^-$ and $[BO_4]^-$-groups. Taking the higher electronegativity of aluminum compared to boron into account, a complete compensation of $[AlO_4]^-$-groups ($3.31\cdot10^{20}$ cm^{-3}) with sodium (and other alkali as well as earth alkali elements) is expected to take place in the first instance. From the total boron concentration of $2.1\cdot10^{21}$ cm^{-3} in Tempax glass and the ratio $[BO_4]^-:[BO_3] = 1:3$ an additional charge compensation of $[BO_4]^-$-groups by Na^+ with a concentration of $5.28\cdot10^{20}$ cm^{-3} has been calculated. The sum of the $[AlO_4]^-$ and the $[BO_4]^-$ concentration agrees with the inventory of the alkali and earth alkali elements in Tempax. Additionally, from the analysis of ^{1}H-^{29}Si-CP (cross polarization) -MAS-NMR and ^{1}H-MAS-NMR spectra was concluded that protons are not incorporated directly or as silanol groups in the bulk glass matrix.

The absence of NBO and hydroxide groups in the bulk glass network, which was proved by the NMR investiga-

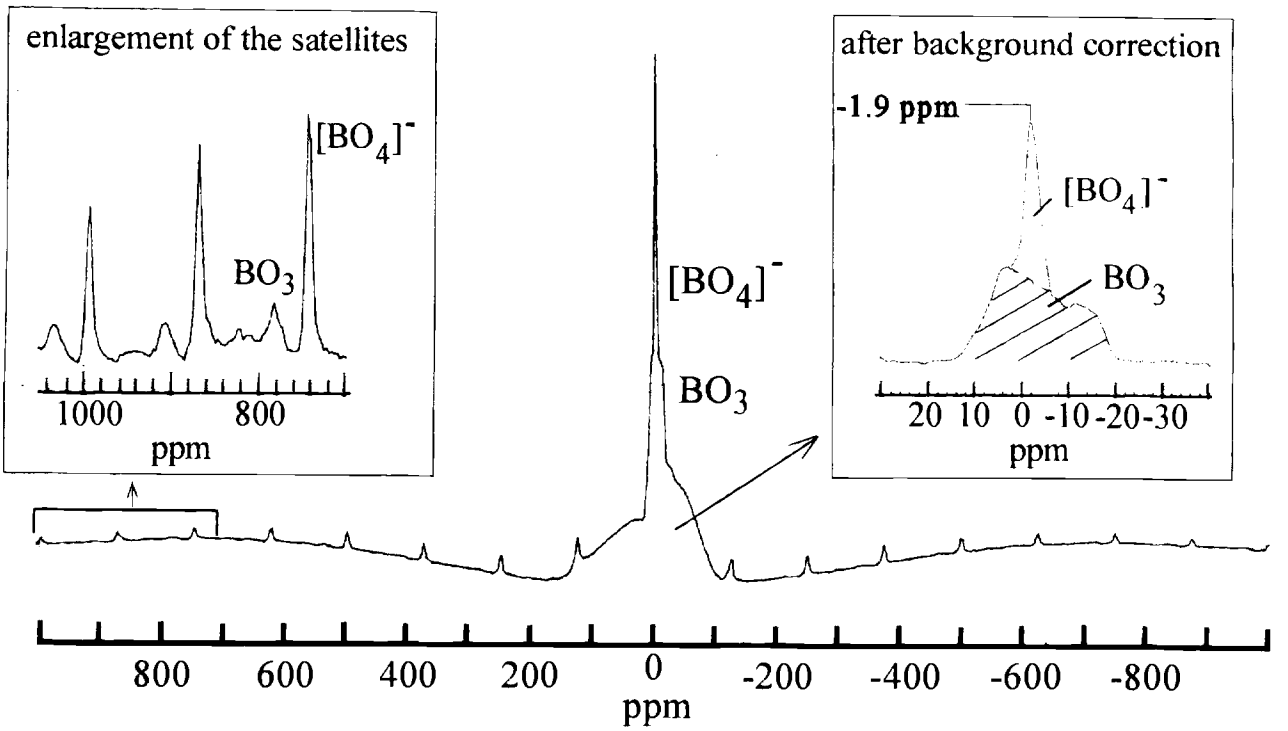

Fig. 8. ^{11}B-MAS-NMR spectra of untreated Tempax glass.

tions suggests an explanation of the oxidation path in anodic bonding that differs from previous models. For the discussion of the oxygen drift and the oxidation process the investigation of the hydrogen drift has proved to be helpful. In all Tempax samples hydrogen could be detected in the near surface region. Corresponding ERDA depth profiles are shown in Fig. 9. For the untreated sample, the H distribution attains a concentration of $(2...3)\cdot10^{21}$ cm^{-3} at its maximum. The measured H inventory can be connected with a modified layer due to the diffusion of H_2O molecules into the glass surface. In the literature this behavior is described by dissolving and leaching effects.[20] The comparison of the H and Na profiles in Fig. 9 shows that the hydrogen drift is coupled to the formation of the sodium depleted polarization layer. As can be seen the initial hydrogen profile redistributes only inside the Na depleted glass layer. The hydrogen (H^-) moves in the same direction as the Na^+ ions. This displacement results in both a hydrogen depletion layer at the glass surface and a pronounced hydrogen profile inside the Na depletion layer. Despite the redistribution of hydrogen inside the Na depletion layer the total hydrogen concentration in the depth up to 800 nm does not change during the given drift sequence. A corresponding statement for depths greater than 800 nm could not be made due to the limited observation depth under the given measurement conditions (incident beam angle $\leq 15°$). Taking into account the strong correlation of the Na and H drift a complete exchange of the weakly bonded Na^+ by H^+ at the $[AlO_4]^-$ and $[BO_4]^-$ network groups inside the depletion layer during the drift process must be assumed. The exchange can be described by the following equilibrium reactions

$$[AlO_4]Na + H^+ \rightleftarrows [AlO_4]H + Na^+ \quad [1]$$

$$[BO_4]Na + H^+ \rightleftarrows [BO_4]H + Na^+ \quad [2]$$

In fact, the drifted Na^+ area density of $0.95\cdot10^{17}$ cm^{-2} is comparable with a H^+ area density of $1.1\cdot10^{17}$ cm^{-2} after a 160 min drift sequence as shown in Fig. 9.

In some cases a hydrogen density pileup was observed at the sodium depletion layer edge, especially at higher temperatures (280°C). This behavior suggests a high activation rate and high mobility of protons only inside the depletion layer. A systematic study of the influence of protons on polarization effects was carried out by Carlson for soda-lime-silica-glasses.[28] A direct comparison with our results is complicated due to the difference in the glass composition but the main evidences are supported.

Assuming that the H_2O dissociation inside the "leached" glass surface layer leads to H^+ and $[OH]^-$ (or, less probably,

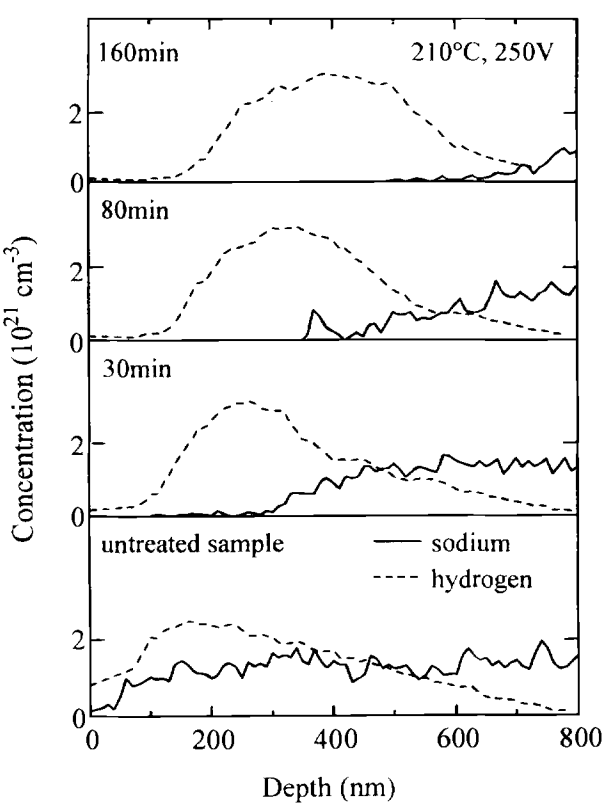

Fig. 9. Correlation between sodium and hydrogen depth profiles in Tempax glass during a drift sequence at T_d = 210°C and U_d = 250 V.

to $[H_3O]^+$ and $[OH]^-$) a displacement of hydroxide groups and, therefore, also of hydrogen toward the anode is expected. Actually, besides the proton drift in the same direction as the Na drift a small shift of the H profile edge toward the anode has been observed at T_d = 240°C, T_d = 280°C, and U_d = 250 V, especially during the initial state of the drift period at $t \leq 1$ min (Fig. 10). The measured amount of drifted oxygen atoms is nearly equal to the number of hydrogen atoms drifted in the same direction. For example, the amount of drifted hydrogen and oxygen toward the anode at T_d = 240°C and U_d = 250 V after 1 min was $3.2 \cdot 10^{15}$ cm^{-2} and $2.83 \cdot 10^{15}$ cm^{-2}, respectively. The assumption of H_2O dissociation in the leached glass surface layer agrees with gas release measurements at the anodic bonding interface,[29] where no water but only oxygen and hydrogen have been observed by quadrupole mass spectrometry.

Summarizing the O drift behavior in Tempax the following chemical interface reaction (oxidation) model is proposed. The drift of the hydroxide groups toward the anode is assumed as the first step. After the $[OH]^-$ drift the hydroxide groups together with the aluminum or silicon atoms build up unstable complexes which can be transformed into metal oxide or silicon oxide and H_2O after the following reaction mechanisms

$$Al + 3\,[OH]^- \rightarrow Al(OH)_3 + 3e^-$$

$$\text{and } 2Al(OH)_3 \rightarrow Al_2O_3 + 3H_2O \quad [3]$$

$$Si + 4\,[OH]^- \rightarrow Si(OH)_4 + 4e^-$$

$$\text{and } Si(OH)_4 \rightarrow SiO_2 + 2H_2O \quad [4]$$

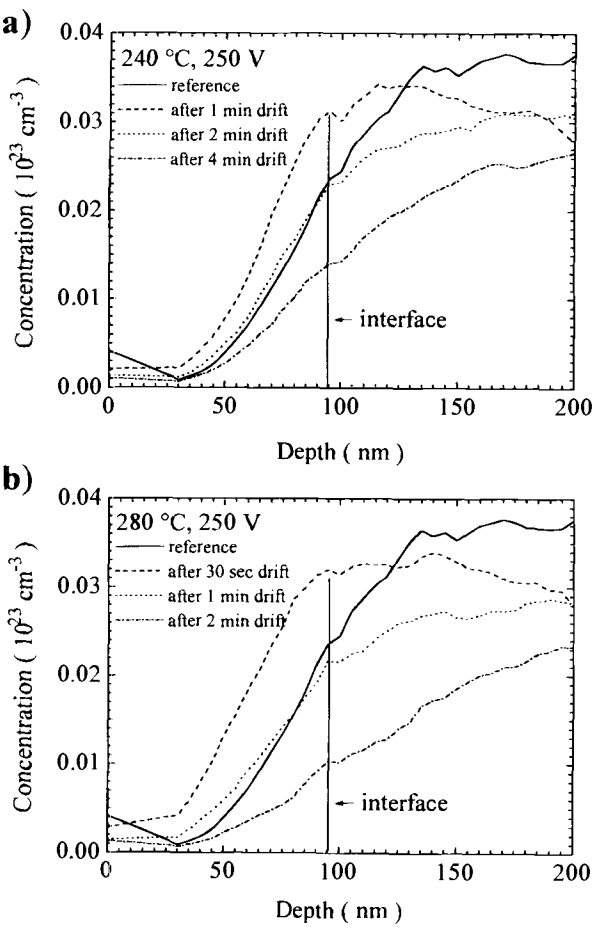

Fig. 10. Drift behavior of hydrogen observed by in situ ERDA at T_d = 240°C (a) and T_d = 280°C (b) during the initial state of a drift sequence with drift voltage of 250 V. At drift times ≤ 1 min the H profile edge is shifted into anode direction.

The earlier supposed model given by Baumann et al.[2] describes the Na_2O dissociation and corresponding drift of $2Na^+$ and O^{2-} toward to the cathode and anode, respectively, that means that the oxygen must exist as NBO in the glass matrix. This explanation of the oxidation mechanism must be revised because the present investigations have shown no evidence for NBO in Tempax.

Conclusion

By means of in situ and ex situ ERDA experiments, the thermally activated alkali drift as the rate dominating process during anodic bonding has been characterized quantitatively. For the Na drift, an activation energy of (0.97 ± 0.14) eV was measured. The Na activation was found to be purely thermal; that is it does not depend significantly on the electric field strength. This corresponds to the results of the NMR investigations, which have shown that Na is mainly ionically bonded to $[AlO_4]^-$ and $[BO_4]^-$ units inside the glass network and only small activation energies are necessary for the Na migration between different bond sites. A nearly ohmic behavior at small depletion layer thicknesses was found for the dependence of the Na drift current on the drift voltage in Tempax glass. The observed saturation effect at increasing depletion layer thicknesses is explained by the decreasing electrical field strength inside the depletion layer. This explanation excludes a significant drift contribution of anions (oxygen) from the bulk glass. Actually, this is consistent with the NMR results, showing that NBO does not exist in the bulk Tempax glass. On the other hand, the leached layer as a source for oxygen is limited and the drift of oxygen saturates already after short drift times. The saturation layer thickness lies in the range of a few micrometers.

Up to now, the importance of hydrogen drift was disregarded in the literature on anodic bonding. In contrast, relatively high concentrations of near surface hydrogen have been established in Tempax by the ERDA investigations. A considerable hydrogen drift was observed only within the Na depletion layer indicating the correlation to the Na drift. Considering the results of the NMR measurements, the weakly bonded Na^+ is completely displaced from the $[AlO_4]^-$ and $[BO_4]^-$ network groups and a temporary exchange by H^+ takes place inside the depletion layer during the drift process. The "leached" glass surface layer acts as a source of H^+, where the hydrogen can exist as H^+ and in form of the chemical compounds $[OH]^-$ or $[H_3O]^+$. Hydrogen and hydroxide groups are absent in the bulk glass.

The results are in contrast to the usual assumption in the literature that the anodic oxidation is the governing chemical reaction mechanism, which would be an activation and drift of oxygen ions in the glass network (NBO) at high electric field strengths. Instead, the presence and the drift of near surface hydroxide groups in Tempax was found to be important. The oxide growth can be related to the drift time by a reciprocal logarithmic equation which describes the oxidation at low temperatures as well as the electrolytical anodic oxidation of metals. Finally, the results indicate an electric field assisted oxide growth supporting the assumption of an anodic oxidation during the anodic metal-glass silicon-glass bonding process.

Acknowledgment

The authors wish to thank Dr. W. Assmann and H. Huber from the Physics Department of the University of Munich for help with the ex situ ERDA measurements at the 14 MV tandem accelerator. This work was supported by the Bundesministerium für Bildung und Forschung (BMBF), Collaborative Project "AN-SYS", Grant No. 13 MV 0266/8.

Manuscript submitted October 14, 1997; revised manuscript received January 16, 1998.

Institut für Ionenstrahlphysik und Materialforschung assisted in meeting the publication costs of this article.

REFERENCES

1. G. Wallis and D. I. Pomerantz, *J. Appl. Phys.*, **40**, 3946 (1969).

2. H. Baumann, S. Mack, and H. Münzel, in *Semiconductor Wafer Bonding: Physics and Applications III*, C. E. Hunt, H. Baumgart, S. S. Iyer, T. Abe, and U. Gösele, Editors, PV 95-7, p. 471, The Electrochemical Society Proceedings Series, Pennington, NJ (1995).
3. A. Cozma and B. Puers, *J. Micromech. Microeng.*, **5**, 98 (1995).
4. D. E. Carlson, K. W. Hang, and G. F. Stockdale, *J. Am. Ceram. Soc.*, **55**, 337 (1972).
5. Y. Kanda, K. Matsuda, C. Murayama, and J. Sugaya, *Sens. Actuators*, **A21-23**, 939 (1990).
6. K. B. Albaugh and D. R. Rasmussen, *J. Am. Ceram. Soc.*, **75**, 2644 (1992).
7. G. Wallis, *J. Am. Ceram. Soc.*, **53**, 563 (1970).
8. D. E. Carlson, *J. Am. Ceram. Soc.*, **57**, 291 (1974).
9. D. E. Carlson, K. W. Hang, and G. F. Stockdale, *J. Am. Ceram. Soc.*, **57**, 295 (1974).
10. M. Toyoda, Y. Fujiya, M. Nayama, and T. Yamada, *Trans. Jpn Welding Soc.*, **24**, 3 (1993).
11. R. G. Gossnik, *J. Am. Ceram. Soc.*, **61**, 539 (1978).
12. J. Goschnick, D. Maas, J. Schuricht, and H. J. Ache, *Fresenius J. Anal. Chem.*, **346**, 323 (1993).
13. M. P. Borom, *J. Am. Ceram. Soc.*, **56**, 254 (1973).
14. D. S. Hurd, R. Caretta, and W. W. Gerberich, *J. Mater. Res.*, **10**, 387 (1995).
15. K. B. Albaugh, *J. Electrochem. Soc.*, **138**, 3089 (1991).
16. S. Grigull, R. Behrisch, U. Kreissig, and M. Harz, *Fresenius J. Anal. Chem.*, **353**, 578 (1995).
17. S. Grigull, U. Kreissig, H. Huber, and W. Assmann, *Nucl. Instr. Methods B*, Submitted.
18. K. Lange, S. Grigull, M. Harz, U. Kreissig, and B. Schmidt, in *Semiconductor Wafer Bonding: Physics and Applications III*, C. E. Hunt, H. Baumgart, S. S. Iyer, T. Abe, and U. Gösele, Editors, PV 95-7, p. 371, The Electrochemical Society Proceedings Series, Pennington, NJ (1995).
19. W. Müller-Warmuth and H. Eckert, *Phys. Rep.*, **88**, 92 (1982).
20. H. Scholz, *Glas - Natur, Struktur und Eigenschaften*, p. 305, Springer Verlag, Berlin (1988).
21. Data sheet of Schröder Spezialglas, Hamburg.
22. C. G. Wilson and A. C. Carter, *Phys. Chem. Glasses*, **5**, 111 (1964).
23. M. Harz, *Sensor Mag.*, **1**, 24 (1995).
24. K. Hauffe, *Oxidation von Metallen und Metallegierungen*, p. 110, Springer Verlag, Berlin (1956).
25. H. Scholz, *Glas - Natur, Struktur und Eigenschaften*, p. 5, Springer Verlag, Berlin (1988).
26. Y. H. Yun and P. J. Bray, *J. Non-Cryst. Solids*, **27**, 363 (1978).
27. M. E. Milberg, J. G. O'Keffe, R. A. Verhelst, and H. O. Hooper, *Phys. Chem. Glasses*, **13**, 79 (1972).
28. D. E. Carlson, *J. Am. Ceram. Soc.*, **57**, 461 (1974).
29. S. Mack, H. Baumann, U. Gösele, H. Werner, and R. Schlögl, *J. Electrochem. Soc.*, **144**, 1106 (1997).

Chemical Diffusion Through Grain Boundaries in Mixed Conductors

J. Jamnik*,[a] and J. Maier*

Max-Planck Institute für Festkörperforschung, 70569 Stuttgart, Germany

ABSTRACT

Chemical diffusion through boundaries involving two charged diffusing species (e.g., O^{2-} and $2e^-$ in an oxide) is modeled taking into account Poisson's equation, restricted to dilute systems and small driving forces. The results are compared with conventional treatments on a single crystal. Grain boundary effects are exemplified for (*i*) a bicrystal containing a grain boundary with adjacent space-charge layers and (*ii*) a polycrystal involving space-charge-free amorphous grain boundaries. Numerical results (*i*) are analyzed in the context of recent experiments on a $SrTiO_3$ bicrystal. Transmission-line approximations for chemical diffusion in polycrystals are proposed and briefly compared with exact results.

Introduction

Chemical diffusion describes how compositional changes propagate in solids. It is a basic process in all chemical reactions involving preparation and corrosion kinetics. In many electrochemical applications, the chemical diffusion coefficient is a decisive materials parameter. It determines, for example, the response time of a conductivity sensor, and the efficiency of an electrochemical filter or an electrode. On the other hand, chemical diffusion can be a decisive mechanistic step in the degradation of electroceramic materials and self-discharge of batteries.

Although chemical diffusion refers to the transport of a neutral component, it is, in ionic compounds, composed of fluxes of at least two charged species (in binary mixed conductors of ions and electrons, e.g., O^{2-} and $2e^-$ for oxygen mass transport). Hence, when compared to electrical conductivity, two additional complications arise: (*i*) at least two different charge carriers (point defects) are always involved and (*ii*) during the course of the transport, stoichiometry of the material changes (at the end of the experiment the sample finds itself in a different state than initially). The concept of chemical diffusion has been well worked out for the electroneutral bulk of single crystals.[1-4] In most applications, however, the materials being studied are polycrystalline, and interfacial kinetics may play a dominant role. In addition, surface processes may not be negligible for the overall kinetics. Surface regions and grain boundaries are usually charged (space-charge layers) and exhibit structural differences (core of the boundary) when compared to the bulk. The equlibrium defect concentrations and possibly also defect mobilities may change very steeply as one is crossing the boundary region. The influence of such concentration gradients on the electrical conductivity has been studied in depth experimentally and theoretically.[5] Regarding chemical diffusion, it is well known that the boundaries play a decisive role, but, surprisingly, there are very few systematic experimental studies and nearly no consistent model available in the literature. Adamcyk and Nowotny[6] focused on surface space-charge effects, but they still neglected perturbation of charge and electric potential within the space-charge layers (single-carrier approximation). Lyubomirsky et al.[7] treated the dopant diffusion through p-n junctions in semiconductors without assuming local electroneutrality, neglecting however the influence of the electrons on the overall transport.

In our laboratory model, experiments were performed using Fe-doped $SrTiO_3$ bicrystals.[8] For this mixed conductor it is generally accepted that grain boundaries are composed of back-to-back Schottky barriers (in the core of

* Electrochemical Society Active Member.
[a] On leave from the National Institute of Chemistry, SI-1000 Ljubljana, Slovenia.